Scripta Materialia 186 (2020) 43–47

Contents lists available at ScienceDirect

Scripta Materialia

journal homepage: www.elsevier.com/locate/scriptamat

# Superelasticity of $(TiZrHf)_{50}Ni_{25}Co_{10}Cu_{15}$ high entropy shape memory alloy

J. Yaacoub[a], W. Abuzaid[b], F. Brenne[a], H. Sehitoglu[a,*]

[a] Department of Mechanical Science and Engineering, University of Illinois at Urbana-Champaign, 1206 W. Green St., Urbana, IL 61801, USA
[b] Department of Mechanical Engineering, American University of Sharjah, PO Box 26666, Sharjah, United Arab Emirates

ARTICLE INFO

*Article history:*
Received 6 March 2020
Revised 2 April 2020
Accepted 15 April 2020
Available online 22 May 2020

*Keywords:*
High entropy alloy
Pseudoelasticity
Shape memory alloy
Multi-component alloy

ABSTRACT

The paper elucidates the superelastic characteristics of high entropy shape memory alloy (HESMA) $(TiZrHf)_{50}Ni_{25}Co_{10}Cu_{15}$ over a wide range of deformation temperatures. Axial compression experiments are presented for different heat treatments and local recoverable strains up to 5% are noted. Superelasticity is observed over a large temperature range up to 175°C. Depending on heat treatment, the critical stress exhibits a Clausius-Clapeyron (CC) slope between 1.4 and 6 MPa/°C up to 80 °C deformation temperature. Obvious deviations from linearity however and significantly higher transformation stresses reaching 1200 MPa are reported at higher temperatures. The temperature change during transformation is reported at 9 °C.



High entropy alloys (HEAs), without a principal element, were originally introduced in the mid-2000s [1–3] but the field was dormant for another ten years. With the lack of a single principle element, these alloys are sometimes referred to as multi-principle element or multi-component alloys. Upon recognition of their exceptional properties, such as high strain hardening coefficients [4–7], high toughness [4], high ductility [4,5,8] and transformation induced plasticity [9], these alloys have received unprecedented attention. The strength-ductility tradeoff is well known in metallurgy, so there is a huge benefit in developing shape memory alloys (SMAs), which are intrinsically brittle, with high entropy characteristics. These new class of shape memory alloys with high entropy characteristics are referred to as HEASMAs.

Early work on HESMAs reported less than 2% recoverable shape memory strain for the $(TiZrHf)_{50}Ni_{25}Co_{10}Cu_{15}$ system [10,11]. The $(TiZrHf)_{50}Ni_{25}Co_{10}Cu_{15}$ is derived from the NiTi system undergoing a B2(cubic) to B19′(monoclinic) transformation [12]. To our knowledge, previous work reported shape memory properties but the superelastic response (i.e. recovery under loading and unloading) of $(TiZrHf)_{50}Ni_{25}Co_{10}Cu_{15}$ has not been explored. In this study, we investigate the superelastic response over a wide range of temperatures, in conjunction with Digital Image Correlation (DIC) measurement of onset of transformation and slip and document the corresponding stress levels from over 20 experiments. We also provide TEM results that unequivocally show the B2-B19' phase transformation and emission of slip into the austenite following reverse transformation. The emission of slip is caused by barriers to martensite motion [13] and influence the functionality of SMAs. We further furnish infrared thermographs demonstrating the transformation-induced temperature changes in these class of alloys which is smaller than conventional SMAs.

The current investigation utilizes compression specimens of square cross section. The samples were electrical discharge machine (EDM) cut from ingots produced in vacuum arc remelting furnace (VAR) using high purity elements. The composition was verified using Inductively Coupled Plasma Spectrometry (ICP) as well as three different Electron Dispersive Spectroscopy (EDS) scans at increasing magnification levels ($4 \times 4$ mm$^2$, $200 \times 200$ μm$^2$ and $40 \times 40$ μm$^2$) from different locations on the specimen as shown in Fig. 1. An EBSD scan confirms the structure to be cubic B2 with an average grain size around 800 microns. The compression specimens had a square cross section of $4 \times 4$ mm$^2$ and a length of 8 mm. Prior to loading, all specimens were polished using SiC paper, after which a fine speckle pattern was applied for full-field strain measurements using Digital Image Correlation (DIC). The back side of the tested specimens were airbrushed with flat black paint to enhance emissivity for Infrared (IR) temperature measurements.

Representative DSC results for three different heat treatments: two solutionizing heat treatments conducted at 1050 °C (including

* Corresponding author.
*E-mail address:* huseyin@illinois.edu (H. Sehitoglu).

https://doi.org/10.1016/j.scriptamat.2020.04.017
1359-6462/

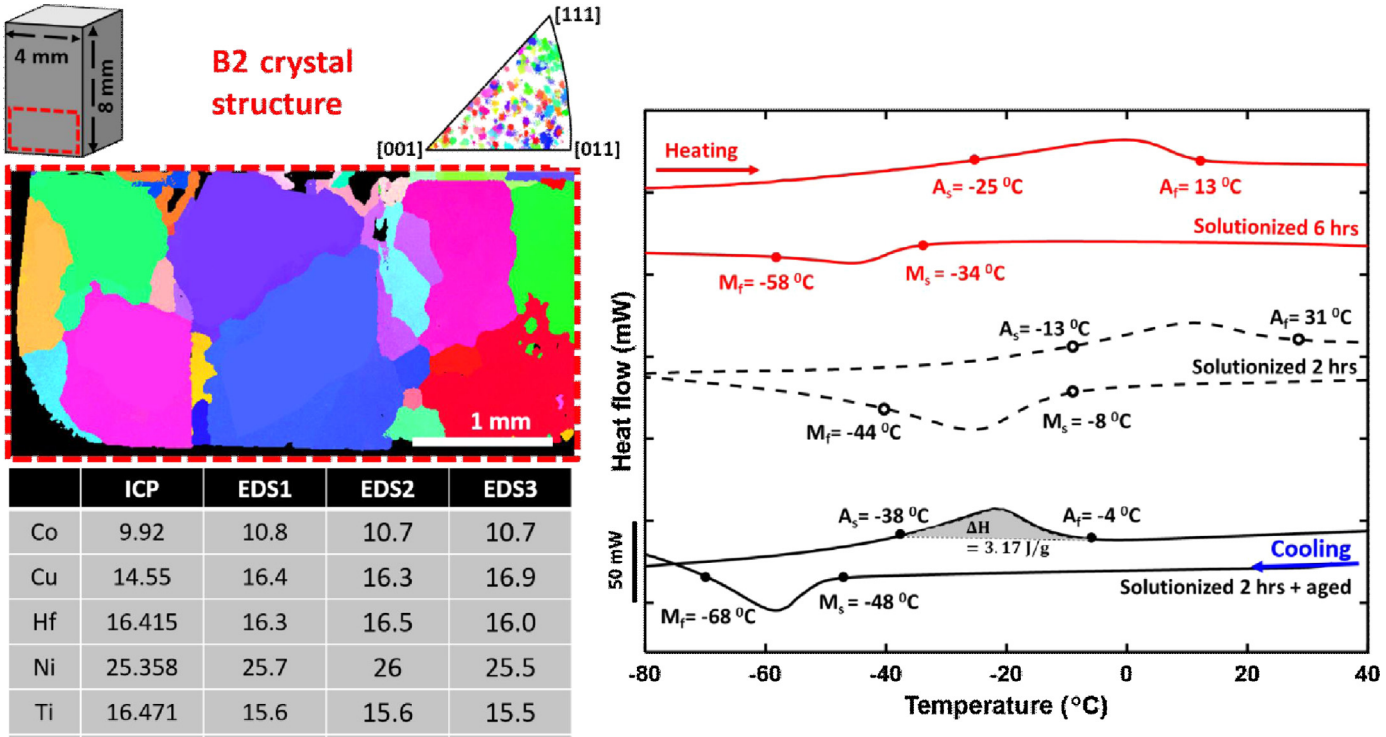


| | ICP | EDS1 | EDS2 | EDS3 |
|---|---|---|---|---|
| Co | 9.92 | 10.8 | 10.7 | 10.7 |
| Cu | 14.55 | 16.4 | 16.3 | 16.9 |
| Hf | 16.415 | 16.3 | 16.5 | 16.0 |
| Ni | 25.358 | 25.7 | 26 | 25.5 |
| Ti | 16.471 | 15.6 | 15.6 | 15.5 |
| Zr | 17.286 | 15.1 | 14.9 | 15.3 |

**Fig. 1.** Sample geometry and EBSD scan of the region indicated with a red rectangle confirming cubic B2 structure, grain size and diversity of grain distribution. The stereographic triangle shown is for the loading direction. The table presents composition results from ICP as well as three different EDS scans along the specimen. DSC scans are presented on the right. The solid black line corresponds to the solutionized for 2 h + aged case. The dashed black line represents the solutionized (2 h) only case and the solid red line the longer 6-h solutionizing treatment. The corresponding characteristic temperatures are marked on the figure. Solutionized only results are scaled up 5 times to aid the eye. DSC heating/cooling rate used was 20 °C/min.

a 450 °C aging heat treatment for 90 min) are depicted in Fig. 1. Prior to solutionizing treatments, the samples were encapsulated in quartz tubes, evacuated, and backfilled with argon to assure an inert environment and prevent oxidation. All heat treatments were terminated by room temperature water quenching following solutionizing. The average enthalpy change is determined to be 2.2 J/g by integration of the heat flow curves for the 3 considered heat treatments.

Uniaxial compression experiments were conducted using a servo-hydraulic load frame at a strain rate of $2 \times 10^{-4}$ $s^{-1}$. Deformation temperatures ranging from −75 °C to 250 °C were achieved through the use of a custom designed liquid nitrogen cooling cell for the lower end of the temperature scale, and heat tape for the upper end. Sample temperature was monitored using a FLIR infrared (IR) camera A6700sc and a thermocouple for cryogenic temperatures. Ample time was allowed before deformation to ensure steady state conditions.

Fig. 2a and b show the stress strain behaviors of $(TiZrHf)_{50}Ni_{25}Co_{10}Cu_{15}$ HEASMA, aged versus unaged, at room temperature and 100 °C, respectively. Both samples were previously solutionized for 2 h at 1050 °C. The solid and dashed black lines represent the global response of the aged and the unaged samples, respectively. Dotted line plots are presented next to the corresponding global curves and reflect the local strains of the sample. Global strains are extracted from the entire test region of the sample for the 'global' response (which would be equivalent to a clip-on extensometer reading). Local strains are extracted from a highly strained zone (martensite band for example) using a custom Area of Interest (AOI) in DIC for the 'local' response. At room temperature, the *aged* sample exhibited superelasticity with local peak strains reaching 5% with full recovery upon unloading (Fig. 2(a)). For the same deformation temperature and applied strain, the *unaged sample* exhibited residual strains of about 1.2% after unloading. Following heating to 200 °C, full strain recovery was observed which is indicative of shape memory behavior. The *unaged* sample exhibited higher strength levels compared to the *aged* case for the same local strain magnitudes (1000 MPa versus 800 MPa at peak). At 100 °C, both *aged* and *unaged* samples exhibited superelasticity with complete strain recoverability. Such a response nearly at $A_f$ +75 °C (Fig. 1) is unprecendented in binary NiTi alloys.

To further elucidate the effect of deformation temperature, the compression response of various specimens was also investigated at temperatures ranging from −75 to 250 °C. Fig. 2c illustrates the stress strain behavior at −75 °C for an aged and an unaged specimen. Shape memory behavior with residual strain recovery occured upon heating. A couple key differences are observed however: first, the attained strength levels for the *aged* sample decreased and the recoverable strains increased in comparison to the *unaged* sample. Secondly, it is evident that the *unaged* sample is stiffer (i.e., has a higher modulus of elasticity) than the *aged* case. While the "apparent" moduli of elasticity [14] for both *aged* and *unaged* cases exhibited a constant magnitude of 75 GPa from room temperature up to 250 °C, the moduli decreased to 30 GPa and 50 GPa respectively for sub room temperature experiments. This measured difference in modulus at lower temperatures is attributed to the twinned and detwinned states of the martensite, [14]. The observed changes at low deformation temperatures are

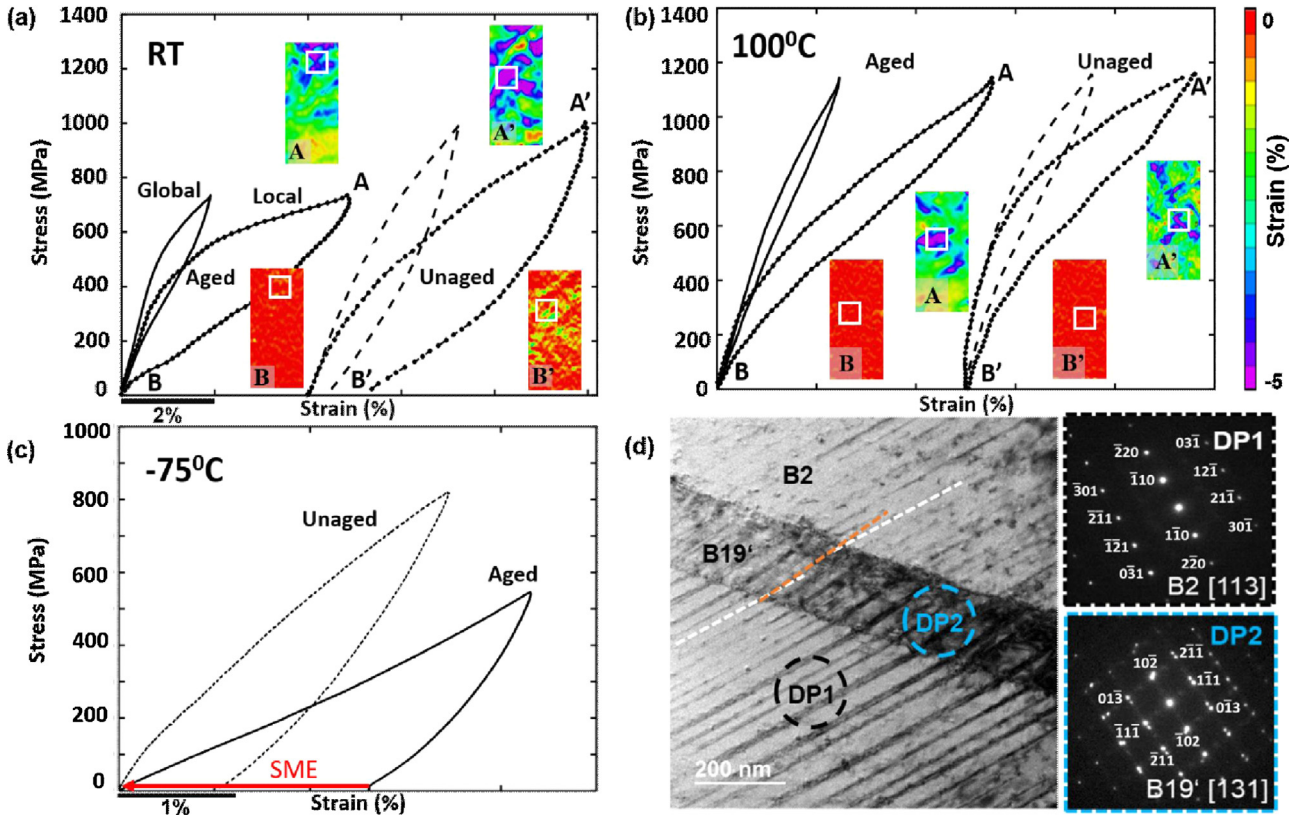


**Fig. 2.** Compressive stress strain behavior of $(TiZrHf)_{50}Ni_{25}Co_{10}Cu_{15}$ in unaged and aged conditions at (a) room temperature and (b) 100 °C, strain scale bar is 2%. The DIC insets cover the entire specimen surface (4 × 8 $mm^2$) and the white boxes indicate the localization area from which local strains were extracted. The compressive stress strain response at −75 °C is shown in (c), strain scale bar is 1%. The TEM bright field image and corresponding diffraction patterns in (d) obtained after compressive testing at room temperature (25 °C) show retained, internally twinned martensite (B19') within the austenitic matrix (B2) and slip emanating from the martensite twins into the austenite.

consistent with the response of NiTi reported earlier [15]. Further studies are needed however to fully explain the effect of aging on precipitate size, transformation temperatures and mechanical response.

Microstructural analyses were conducted after mechanical testing at room temperature (25 °C) using a TEM JEOL 2010 operating at 200 kV. The specimen was prepared via FIB using a FEI Scios 2 dual beam system following standard preparation techniques. The bright field image obtained from a [113] zone axis is given in Fig. 2d. The diffraction patterns obtained from the regions marked with DP1 and DP2 in Fig. 2d are given as insets. The presence of retained martensite (major dark feature, DP2) within the austenitic matrix (brighter area, DP2) is evident from the real image as well as the diffraction pattern. Additionally, both areas show almost parallel bands only several micrometers in width. However, a difference in the orientation of these features within the martensite versus the austenite is noted, as highlighted by the dashed white and orange lines. Furthermore, the diffraction pattern of the martensite (DP2) illustrates the presence of twins while this is not the case for the austenite (DP1). These findings demonstrate: (a) the internally twinned nature of the martensite and (b) dislocation emission from the martensitic twin interfaces into the austenite. The latter is further supported by the decreasing slip band width within the austenite when moving away from the A-M interface. The individual slip bands fade out and do not proceed throughout the entire TEM specimen. We confirm this by observing an area further away from the interface where a lower slip band density and width is noted. This is similar to the observations previously reported in Cu-Zn and FePt alloys [16,17], where it was proposed that twinning dislocations produce an 'emissary dislocation' into the austenite emanating from the interface (reverse transformation) [13,18]. The proposed dislocation reactions were summarized for earlier for NiTi, and the possible advantage of HESMAs (with higher strength compared to NiTi and others) could be to accommodate the misfit at interfaces with elastic distortions.

The critical flow stresses are presented in Fig. 3. A Clausius-Clapeyron slope range of 1.4 for a lower bound and 6 MPa/°C for an upper bound is proposed in the superelastic range. The curves however exhibit a non-linear response at higher temperature ranges: the critical stress (around 1250 MPa) deviates from the initial proportional trend. In fact, superelasticity is still observed at higher temperatures, in conjunction with plastic flow, up to 150 °C. This behavior has been observed for other SMAs (such as NiTi, $NiTiHf_{13.3}$, $Ni_2FeGa$, NiTiCu or CuZnAl) [19] but the non-linearity in stress-temperature curve is more pronounced for the HEASMA. Also, superelasticity at stress levels near 1200 MPa has only been achieved with NiTiHf alloys [20] to our knowledge.

The release (or absorption) of latent heat associated with the martensitic transformation [19,21] is well known. Its consequences are: increase in stress hysteresis, increase in max. stress under strain control which are all detrimental to fatigue response. By using a double-ramp loading scheme (the unloading process is performed at a much faster strain rate of 0.1 $s^{-1}$ to simulate adiabatic conditions) a measure of temperature change was established as 10 °C in Fig. 4. This change can be determined using the following: $\Delta T_{th} = -\frac{T}{C_p}\Delta S$, $\Delta S = \frac{\Delta H}{T_0}$, $T_0 = \frac{1}{2}(M_s + A_f)$ where $\Delta T_{th}$ is the the-

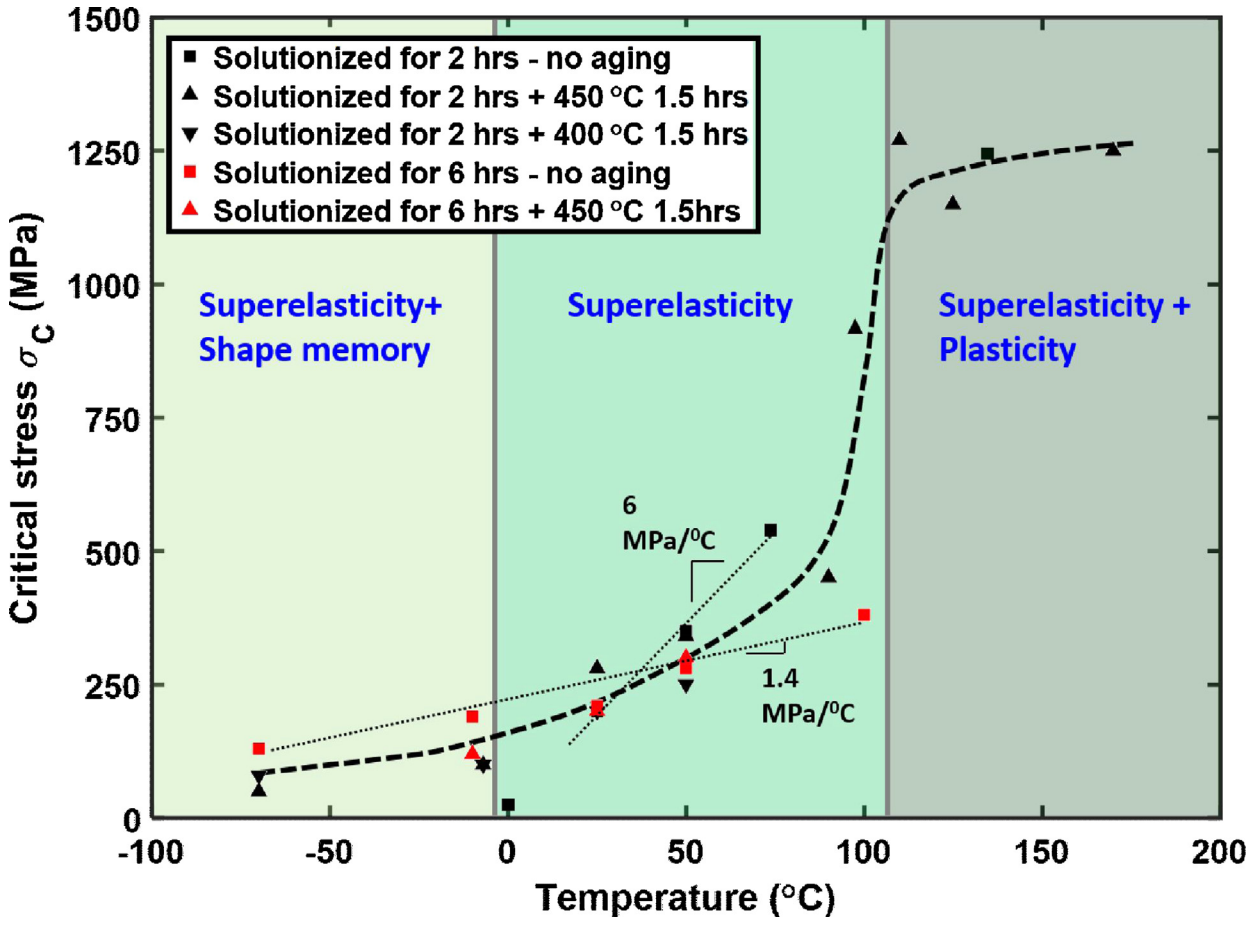


**Fig. 3.** Flow stresses as a function of temperature for $Ti_{16.67}Zr_{16.67}Hf_{16.67}Ni_{25}Co_{10}Cu_{15}$. The Clausius-Clapeyron slope is in the range of 1.4 MPa/°C for a lower bound and 6 MPa/°C for and upper bound and is indicated on the figure.

oretical temperature change during transformation, $T$ is the testing temperature (room temperature in this case), $C_p$ is the specific heat capacity of the alloy, $\Delta S$ is the entropy change, $T_0$ is a reference temperature as described in [22], $\Delta H$ the enthalpy change of the phase transformation (2.2 J/g as determined from DSC). The specific heat was determined using the ASTM E2716 standard as 265 $J/Kg^{-K}$. Accordingly, the entropy change of the martensitic transformation is determined as $-8.9$ $J/Kg^{-K}$, which is the lowest of the reported values for other well-known shape memory alloys- such as NiTi at $-52$, CuZnAl at $-23.5$, $Ni_2FeGa$ at $-19.5$, $NiTiHf_{13.3}$ at $-59$ and NiTiCu at $-38$ $J/Kg^{-K}$ [19]. Such a small entropy change may have beneficial consequences in high rate deformations where large changes in temperature have been measured with attendant deterioration of superelasticity [23]. The theoretical temperature change $\Delta T_{th}$ was determined at 10 °C (upon substitution to above formulas), in excellent agreement with the experimentally measured value of 9.6 °C. Temperature changes measured were substantially lower (~1 °C) in the plastic regime consistent with the literature [24].

In summary, the potential benefits of $(TiZrHf)_{50}Ni_{25}Co_{10}Cu_{15}$ are numerous: high transformation stresses, a wide superelastic temperature range (>100 °C encompassing room temperature compared to NiTi (≈30 °C) [25]) and small levels of transformation induced- temperature change which can impart favorable fatigue properties [26]. The high transformation stress levels are also of particular interest as they allow for large work output.

Overall, the work supports the following conclusions:

1. Depending on the deformation temperature, both superelastic and shape memory properties have been demonstrated for high entropy shape memory alloy $Ti_{16.67}Zr_{16.67}Hf_{16.67}Ni_{25}Co_{10}Cu_{15}$. Based on the different heat treatments considered in this work, the transformation temperatures, and consequently SE and SM temperature ranges, can be potentially tailored for specific application requirements. The difference between the local (transformation capacity) and global strain levels points to potential benefits from textured and single crystalline versions of HESMA. Further research is needed to fully understand the effect of heat treatment on the microstructure and behavior of this HESMA.
2. Based on the TEM results, slip lines emanating from the A-M interface into the austenite matrix are noted. The origin of slip emission has been studied in recent work and this alloy (with six elements) can be further optimized to minimize inherent slip-induced irreversibilities.
3. The relatively low entropy change and consequently low temperature change during transformation points much lower sensitivity to frequency effects in fatigue commonly observed in other shape memory alloys. This lower temperature change could also impart a smaller stress hysteresis upon optimizing the composition.

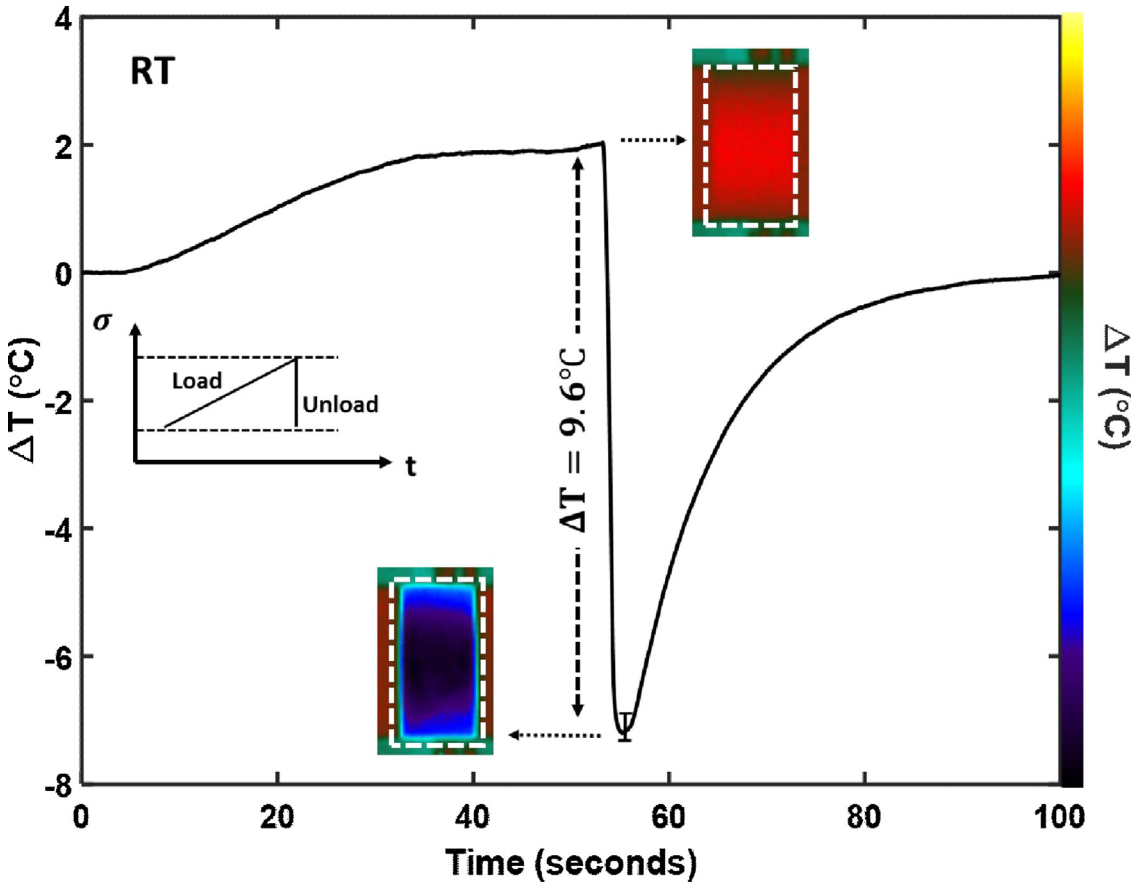


**Fig. 4.** Infrared IR temperature signature during an asymmetric double ramp loading (the inset shows slow loading and rapid unloading) cycle for an *aged* sample at room temperature for $Ti_{16.67}Zr_{16.67}Hf_{16.67}Ni_{25}Co_{10}Cu_{15}$. Color scale bar on right hand side corresponds to the same $\Delta T$ scale on left side of the figure. Multiple tests were conducted and the error bar shows the variation.

## Declaration of Competing Interest

The authors declare that they have no known competing financial interests or personal relationships that could have appeared to influence the work reported in this paper.

## Acknowledgments

The work is supported by National Science Foundation DMR grant 1709515 Metallic Materials and Nanomaterials Program. The EBSD analyses were carried out in part in the Frederick Seitz Materials Research Laboratory Central Research Facilities, University of Illinois.

## References

[1] B. Cantor, I.T.H. Chang, P. Knight, A.J.B. Vincent, Mater. Sci. Eng. 375–377 (2004) 213–218.
[2] J.-W. Yeh, S.-K. Chen, S.-J. Lin, J.-Y. Gan, T.-S. Chin, T.-T. Shun, C.-H. Tsau, S.-Y. Chang, Adv. Eng. Mater. 6 (5) (2004) 299–303.
[3] C.-J. Tong, Y.-L. Chen, J.-W. Yeh, S.-J. Lin, S.-K. Chen, T.-T. Shun, C.-H. Tsau, S.-Y. Chang, Microstructure , Metall. Mater. Trans. A 36 (4) (2005) 881–893.
[4] B. Gludovatz, A. Hohenwarter, D. Catoor, E.H. Chang, E.P. George, R.O. Ritchie, Science 345 (6201) (2014) 1153–1158.
[5] Z. Li, K.G. Pradeep, Y. Deng, D. Raabe, C.C. Tasan, Nature 534 (7606) (2016) 227–230.
[6] W. Abuzaid, H. Sehitoglu, Mater. Char. 129 (2017) 288–299.
[7] S. Alkan, A. Ojha, H. Sehitoglu, Acta Mater. 147 (2018) 149–164.
[8] D. Li, C. Li, T. Feng, Y. Zhang, G. Sha, J.J. Lewandowski, P.K. Liaw, Y. Zhang, Acta Mater. 123 (2017) 285–294.
[9] Z. Li, C.C. Tasan, K.G. Pradeep, D. Raabe, Acta Mater. 131 (2017) 323–335.
[10] G. Firstov, T. Kosorukova, Y.N. Koval, V. Odnosum, Mater. Today 2 (2015) S499–S503.
[11] G.S. Firstov, T.A. Kosorukova, Y.N. Koval, V.V. Odnosum, Mater. Today 2 (2015) S499–S503.
[12] G. Firstov, A. Timoshevski, T. Kosorukova, Y. Koval, Y. Matviychuk, P. Verhovlyuk, MATEC Web Conf. 33 (2015) 6006.
[13] A.S.K. Mohammed, H. Sehitoglu, Acta Mater. 186 (2020) 50–67.
[14] J. Wang, H. Sehitoglu, Int. J. Plast. 61 (2014) 17–31.
[15] H. Sehitoglu, I. Karaman, R. Anderson, X. Zhang, K. Gall, H.J. Maier, Y. Chumlyakov, Acta Mater. 48 (13) (2000) 3311–3326.
[16] S. Kajiwara, T. Kikuchi, Acta Metall. 30 (2) (1982) 589–598.
[17] S. Kajiwara, W.S. Owen, Metall. Trans. 5 (9) (1974) 2047–2061.
[18] A.S.K. Mohammed, H. Sehitoglu, Acta Mater. 183 (2020) 93–109.
[19] Y. Wu, E. Ertekin, H. Sehitoglu, Acta Mater. 135 (2017) 158–176.
[20] H. Sehitoglu, Y. Wu, L. Patriarca, G. Li, A. Ojha, S. Zhang, Y. Chumlyakov, M. Nishida, Shape Memory Superelast. 3 (2) (2017) 168–187.
[21] L. Mañosa, A. Planes, Philos. Trans. R. Soc. A 374 (2074) (2016) 20150310.
[22] H.C. Tong, C.M. Wayman, Acta Metall. 22 (7) (1974) 887–896.
[23] S. Nemat-Nasser, J.-Y. Choi, W.-G. Guo, J.B. Isaacs, Mech. Mater. 37 (2) (2005) 287–298.
[24] G.I. Taylor, H. Quinney, Proc. R. Soc. Lond. Ser. A 143 (849) (1934) 307–326.
[25] K. Otsuka, C.M. Wayman, Shape Memory Materials, Cambridge university press, 1999.
[26] Y. Zhang, Y. You, Z. Moumni, G. Anlas, J. Zhu, W. Zhang, Int. J. Plast. 90 (2017) 1–30.